Results in Physics 5 (2015) 28–31

Contents lists available at ScienceDirect

Results in Physics

journal homepage: www.journals.elsevier.com/results-in-physics

Generation and characterization of point defects in $SrTiO_3$ and $Y_3Al_5O_{12}$

F.A. Selim [a,b,*], D. Winarski [a], C.R. Varney [c], M.C. Tarun [c], Jianfeng Ji [a,c], M.D. McCluskey [c]

[a] Physics Department, Bowling Green State University, Bowling Green, OH 43403, USA
[b] Center for Photochemical Sciences, Bowling Green State University, Bowling Green, OH 43403, USA
[c] Physics Department, Washington State University, Pullman, WA 99164, USA

ARTICLE INFO

Article history:
Received 14 December 2014
Accepted 14 January 2015
Available online 22 January 2015

Keywords:
Complex oxides
Strontium titanate
Garnets
Positron annihilation spectroscopy
IR spectroscopy
Point defects

ABSTRACT

Positron annihilation lifetime spectroscopy (PALS) was applied to characterize point defects in single crystals of $Y_3Al_5O_{12}$ and $SrTiO_3$ after populating different types of defects by relevant thermal treatments. In $SrTiO_3$, PALS measurements identified Sr vacancy, Ti vacancy, vacancy complexes of Ti–O (vacancy) and hydrogen complex defects. In $Y_3Al_5O_{12}$ single crystals the measurements showed the presence of Al-vacancy, (Al–O) vacancy and Al-vacancy passivated by hydrogen. These defects are shown to play the major role in defining the electronic and optical properties of these complex oxides.

Introduction

Defects have profound effects on the structural and electronic properties of materials. Complex oxides in particular exhibit a high level of native defects because of their structure complexity and deviations from stoichiometry. This makes most of their properties defined by the type and level of defects in the lattice. Here we study lattice defects in two complex oxides, yttrium aluminum garnet $Y_3Al_5O_{12}$ (YAG) which has the garnet structure and Strontium titanate $SrTiO_3$ which has the perovskite structure. Both of these two oxides have great technological importance. YAG is the host material for most solid state lasers and many phosphors and scintillation materials and reference therein [1,2]. $SrTiO_3$ on the other hand exhibits a variety of interesting phenomena such as ferro-electricity, superconductivity and ferromagnetism and it has great potential for oxide based devices [3,4].

We have recently shown that point defects lead to interesting phenomena in both YAG and $SrTiO_3$ bulk materials. In YAG, hydrogen related defects have led to significant band gap narrowing and substantially alter the optical and scintillation properties of YAG crystals [5]. In $SrTiO_3$ we reported two orders of magnitude persistent photoconductivity (PPC) at room temperature originated by point defects in the lattice [6]. This level of PPC at room temperature has never been reported in any system before. Accordingly, it is important to investigate how to populate and characterize point defects in complex oxides. Positron annihilation spectroscopy is a versatile unique tool for studying vacancy defects [7,8]. It is based on implanting positrons in the sample and measuring the 511 keV annihilation photons. These photons carry information about electron states in the solid with which the positrons annihilate and they can be measured by positron lifetime, Doppler broadening or angular correlation methods [7–11]. The detection of defects by positrons is based on the fact that positrons may be trapped by open volume defects. This is because a positron is strongly repelled by ion cores in the lattice due to their positive charge. The absence of a positive charge in a vacancy provides an attractive potential that traps positrons at this site, and this trapping leads to significant changes in the measured positron annihilation parameters. As the vacancy lacks the electrons of the missing atom, the electron density is lower leading to a longer positron lifetime. In this work we applied positron annihilation lifetime spectroscopy (PALS) as it gives the most detailed information about defects, revealing their structures and sizes. One major advantage of PALS is its capability in revealing the structure of complex defects. We also applied Fourier Transfer Infrared (FTIR) spectroscopy [12] in combination with PALS to study the local vibration of hydrogen related defects in the YAG structure.

Experimental details

PALS measurements have been carried out using a conventional coincidence lifetime spectrometer, with a Na-22 positron source.

* Corresponding author at: Physics Department, Bowling Green State University, Bowling Green, OH 43403, USA.
E-mail address: faselim@bgsu.edu (F.A. Selim).

http://dx.doi.org/10.1016/j.rinp.2015.01.002
2211-3797/

The spectrometer was located earlier at Washington State University and later at Bowling Green State University. The source emits a 1.27 MeV γ-quantum that is time-coincident with the creation of each positron in decay of Na-22. The positron lifetime is measured as the time difference between the detection of the 1.27 MeV photon and one of the two 0.511 MeV photons emitted from the positron annihilation event in the material. The delayed time-coincidence lifetime spectrometer is built from two scintillation detectors using BaF_2 detectors, two constant fraction discriminators, a time-to-amplitude converter and an analog-to-digital pulse-height converter. The positron source was prepared by depositing NaCl on 8 micron-thick Kapton foil, then folded and sandwiched between two identical samples. Lifetime spectra were recorded with three million coincidences accumulated for good statistics. The timing resolution of the system was about 200 ps. The spectra were fitted using PATFIT program and reference therein [13,14]. Each measured lifetime spectrum for $SrTiO_3$ or YAG samples was analyzed as a superposition of exponential decay components convoluted with the instrumental resolution function. Decay components due to positron annihilation in the source were subtracted from the spectra, one component with 384 ps lifetime and 10% intensity from the Kapton foil and another with 430 ps lifetime and 1% intensity from NaCl. If the concentration of defects that trap positrons is sufficiently low, we obtain only a single lifetime component after subtracting the source correction. This lifetime corresponds to the bulk lifetime τ_B which is characteristic of positron annihilation in the bulk of the material. Two lifetime components gave the best fit for most measurements, τ_2 which represents the characteristic defect lifetime and τ_1, which is reduced from τ_B by an amount that depends on the rate of positron trapping to the defect.

IR absorption measurements were performed at Washington State University using a Bomem DA8 Fourier transform infrared spectrometer with a globar light source, a KBr beam splitter, and a liquid nitrogen-cooled InSb detector. Measurements were performed at both room temperature and 10 K. Samples were maintained at liquid-helium temperatures (~10 K) in a Janis continuous-flow cryostat. The spectral range of the spectrometer covers from 1800 to 7000 cm^{-1} and its resolution is 0.2 cm^{-1}.

PALS measurements were carried out on as-received and annealed $SrTiO_3$, undoped YAG and Ce-doped YAG single crystals. $SrTiO_3$ samples were provided from MTI Inc. and Maktec. YAG samples were grown at Crytur Inc., Czech Republic. A number of samples were further annealed in different environments to populate different types of defects as described below. IR measurements were carried out on a number of undoped and Ce doped YAG crystals.

Results and discussion

$SrTiO_3$

To populate different types of defects in $SrTiO_3$, single crystals were annealed in SrO, TiO_2 and hydrogen atmospheres. They were annealed in an evacuated ampoule filled with SO or TiO_2 at 1200 °C for 1 h. PALS spectra were recorded from as-received and annealed samples and analyzed using PATFIT program and the one-defect trapping model. Table 1 presents the reduced positron lifetime τ_1, characteristic defect positron lifetime value τ_2, the defect intensity I_2 and the proposed defect type for each sample. Thanks to the previous theoretical and experimental works by Keeble et al. on $SrTiO_3$ [15–17], interpretation of PALS data for $SrTiO_3$ samples is straight forward. In our current measurements, as-grown samples received from different suppliers have different defect lifetime τ_2. This has been observed before in $SrTiO_3$ single crystals measured by Mackie and co-workers [17]. In Table 1, the as-received samples from MTI Inc. (sample #1) displayed in row 1 showed τ_2 of 185 ps indicating the presence of Ti vacancy. After annealing them in SrO τ_2 has increased to 210 ps (sample #1 displayed in row 2). We assign the 210 ps value to unresolved lifetimes of Ti vacancy and Ti–O vacancy. SrO anneal probably extracts oxygen atoms from $SrTiO_3$ lattice and forms SrO_2. This led to the formation of O-vacancies next to Ti-vacancies, i.e. (Ti–O) di-vacancies which have positron lifetime between 225 and 239 ps [17]. Anneal in TiO_2, on the other hand, did not change the defect lifetime. The 222 ps τ_2 in the as-received and annealed samples from MakTec (samples #2 and #3 displayed in row 3 and 4) corresponds to a combination of Sr-vacancy and Ti-vacancy [17]. Hydrogen anneal (see samples #4 and #5) led to the formation of complex defects, probably in the form of vacancy clusters as indicated by the long defect lifetime 279 and 315 ps. This long lifetime associated with hydrogen complex defects has been previously observed in other semiconductors [18].

The formation of (Ti–O) after annealing in SO has led to two orders of magnitude persistent photoconductivity (PPC) in $SrTiO_3$ single crystals. This PPC was observed by an increase in free carrier concentration and then confirmed by an increase in charge carrier concentration and conductivity through Hall-effect measurements as discussed in Ref. [6]. This level of PPC in bulk materials has never been observed at room temperature in any system [19,20]. It reflects the significant role of point defects in defining the electronic properties of materials.

$Y_3Al_5O_{12}$

PALS measurements were performed on YAG single crystals grown in Ar, O, and H atmospheres; their positron decay curves are shown in Fig. 1. It is obvious from their decays that YAG grown in Ar exhibits much longer lifetime, while H-grown sample exhibits shorter decay curve and can be fitted to single line, which indicates the presence of one lifetime component. Table 2 presents the lifetime values and intensities for each sample. Fig. 2 compares the lifetime spectra for as-grown and annealed samples. As seen in the graphs in Figs. 1 and 2, the spectra arising from annihilation in H-grown samples fit very well to one lifetime component indicating the absence of positron traps. However after annealing the H-grown sample in air for 48 h (Fig. 2 and Table 2), a second positron lifetime component appears. This is probably because anneal in air reduced the hydrogen concentration leading to partial positron trapping. The large uncertainty in I_2 after annealing in air

Table 1
PALS results for as-received and annealed $SrTiO_3$ single crystals.

#	Sample	τ_1 (ps)	τ_2 (ps)	I_2%	Proposed defect type
1	As-received from MTI	120(3)	185(3)	50(4)	Ti-vacancy
1	Annealed in SrO From MTI	143(2)	210(6)	27(5)	Ti-vacancy (Ti–O)vacancy
2	As-received from Mateck	128(3)	220(5)	35(4)	Sr-vacancy Ti-vacancy
3	Annealed in TiO_2 from Mateck	125(2)	217(2)	40(2)	Sr-vacancy Ti-vacancy
4	Annealed in H from MTI	143(1)	279(6)	15(1)	Hydrogen vacancy complexes
5	Annealed in H from MTI, different batch	153(1)	315(6)	15(1)	Hydrogen vacancy complexes

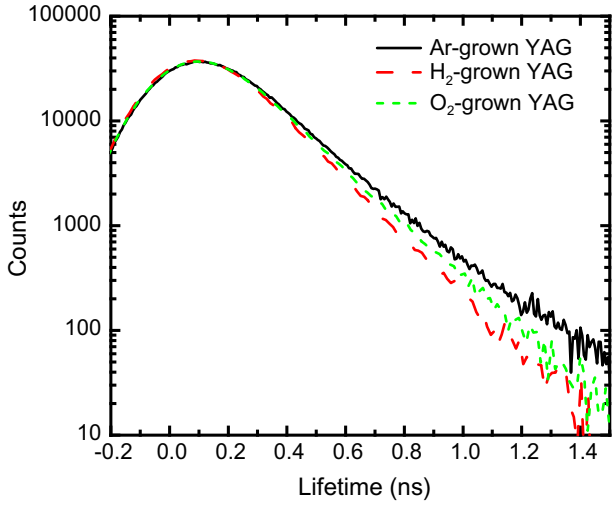

Fig. 1. Lifetime spectra of as-grown YAG single crystals grown in Ar-, O-, and H-atmospheres.

Table 2
PALS results for as-grown and annealed YAG single crystals.

Sample	τ_1 (ps)	τ_2 (ps)	I_2%	Proposed defect type
Ar-grown	157(2)	279(11)	13(2)	(Al–O) vacancy
O-grown	160(3)	249(15)	6(1)	Al-vacancy
H-grown	152(0.1)			None
H-grown annealed in air	147(0.3)	236(39)	6 (4)	Al-vacancy

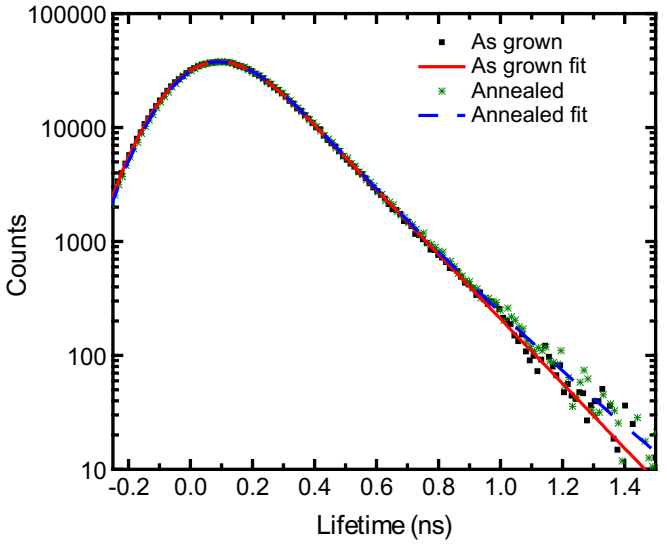

Fig. 2. Lifetime spectra of H-grown samples (as-grown) and after air-anneal for 48 h. A second lifetime appears in the sample after annealing.

is due to the close values between τ_B and τ_2 and the difficulty of resolving them in the spectrum. However the variance of the fit is around 1.0 and the fit definitely showed two lifetime components. The absence of second lifetime and positron trapping in H-grown samples does not mean the absence of defects in these crystals; but it indicates passivation of vacancies by hydrogen which prevent positron trapping. In fact, it is impossible to grow defect-free YAG single crystals because of the non-stoichiometry and the very high temperature required for the growth process. After annealing in air at high temperature for long time, some hydrogen atoms diffused out of the vacancies leading to positron trapping.

The defect lifetime, τ_2, is 279(11) ps for Ar-grown samples and 249(15) ps for O-grown samples. The 249 ps lifetime is a common value for Al mono-vacancy in many systems. Therefore we assign it to single Al vacancy and the 279 ps to Al–O vacancy as explained in Ref. [9]. By annealing Ar-grown YAG sample in O-atmosphere, τ_2 reduced from 279 to 256 ps, which is probably because of filling oxygen vacancies. This supports the association of the 279 ps lifetime with (Al–O) vacancy.

PALS measurements were also carried out on Ce doped YAG samples grown in Ar or H atmosphere. Ce doped YAG cannot be grown in O-atmosphere as the oxidizing atmosphere prevents the formation of Ce^{3+}. In Ar-grown samples, τ_2 is quite long (305 ps) which is an indication for the presence of large vacancy clusters. However τ_2 is absent in all Ce doped YAG samples grown in hydrogen indicating the absence of positron traps and confirming hydrogen passivation of cation vacancies observed in the undoped crystals. Anneal of H-grown Ce doped YAG samples in air did not lead to a significant change in PALS measurements. With respect to Ar-grown samples, anneal in O-atmosphere reduced the defect density I_2 but did not substantially affect the value of τ_2. A few samples were annealed in nitrogen atmospheres, however no effect on PALS data has been observed.

It is interesting to observe the complete absence of positron trapping in all undoped and doped YAG crystals grown in H-atmosphere in this work and in our previous work [9] despite the high level of defects that are always present in the YAG structure and the deficiency of aluminum [9]. Infrared (IR) absorption spectra can provide some information about hydrogen incorporation in the structure. Earlier, we have carried Fourier Transform Infrared (FTIR) measurements on H- and O-grown YAG single crystals at liquid helium temperature [9]. In this study we follow with FTIR measurements of undoped and Ce doped YAG crystals at room temperature. Fig. 3 shows the IR absorption spectra for O-grown YAG samples at room and liquid helium temperatures. Two peaks were identified at 3335 and 3370 cm^{-1} at liquid helium temperature. These values were reported to be associated with O–H stretching vibrational modes [21]. They represent hydrogen atoms located at two different interstitial sites. For H-grown samples, previous measurements presented in Ref. [9] showed a peak at 3416 cm^{-1} at liquid helium temperature. The emergence of this

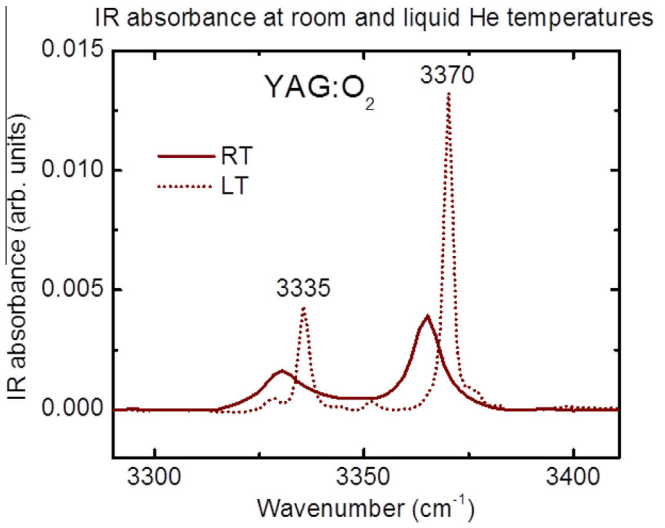

Fig. 3. FTIR absorption measurements of YAG single crystal grown in O-atmosphere at liquid helium and room temperatures.

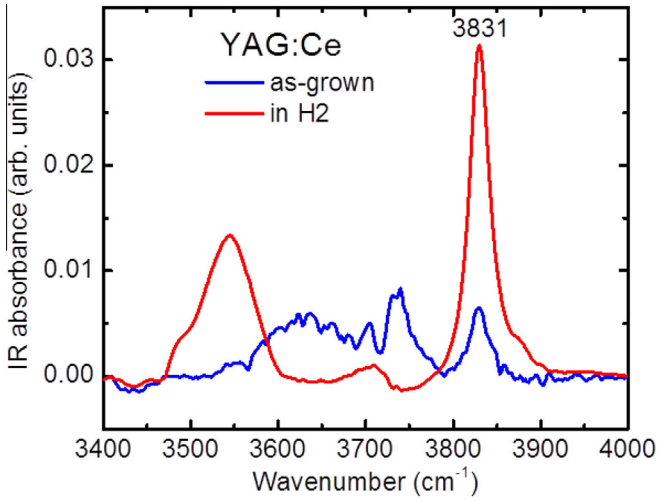

Fig. 4. FTIR absorption measurements of Ce-doped YAG single crystal grown in H-atmosphere at room temperature.

higher frequency peak in H-grown samples is a sign for the incorporation of hydrogen in the structure in a different mode, probably inside a vacancy [12]. In Fig. 3, the difference in peak position and Full width at half maximum (FWHM) between liquid helium and room temperature is due to the considerable temperature dependence of IR peaks [22].

The IR absorption measurements in Fig. 4 represent the first vibrational spectroscopy study for Ce doped YAG. It shows a strong peak at 3831 cm^{-1}. The origin of this peak is not known as there is no previous experimental or theoretical vibrational spectroscopy study for Ce doped YAG crystals. However the presence of this peak in H-grown Ce doped YAG sample only suggests its association with Ce–H bond. A possible scenario for the formation of this peak is as follows. Ce replaces a yttrium atom in the YAG lattice and forms bonds with hydrogen atoms inside the Al vacancy.

We should mention that this incorporation of hydrogen in the YAG structure has great effect on the electronic and optical properties of YAG single crystals. First, it leads to significant band gap narrowing (BGN) as proven experimentally and theoretically [5]. Second, it eliminates all exciton traps in the YAG structure which has been observed by the complete absence of thermoluminescence in YAG crystals grown in hydrogen atmosphere [5]. The change of the defect structures and the subsequent induced phenomena in both YAG and $SrTiO_3$ is not only in the surface regions but it extends to the bulk of the materials. This is because the mean penetration depth of positrons emitted from Na-22 – the source used in the current experiment – is 100 microns which provides bulk measurements with negligible contribution from positron annihilation at the surface. Accordingly the measurements here reflect the change in the defect structure in the bulk.

Conclusion

Different types of point defects have been populated in $SrTiO_3$ and $Y_3Al_5O_{12}$ complex oxides by relevant thermal treatments. PALS provided evidence for the presence of these defects and enabled their characterization at the atomic level. The quality of semiconductor materials is often limited by the presence of electronically active point defects. It is interesting to see how point defects in $SrTO_3$ enhance the conductivity and induce very high level of photoconductivity and how they lead to new phenomena in complex oxides.

Acknowledgements

We acknowledge receiving funds from NSF/DMR1359523 grant (Charles Ying) and DOE Grant No. DE-FG02-07ER46386.

References

[1] Zych E, Brecher C, Glodo J. J Phys Condens Matter 2000;12:1947.
[2] Varney C, Mackay T, Pratt A, Selim F. J Appl Phys 2012;2012(111):063505.
[3] Son J, Moetakef P, Jalan B, Bierwagen O, Wright N, Engel-Herbert R, Stemmer S. Nat Mater 2010;9:482.
[4] Kan D, Terashima T, Kanda R, Masuno A, Tanaka K, Chu S, Kan H, Ishizumi A, Kanemitsu Y, Shimakawa Y, Takano M. Nat Mater 2005;4:816.
[5] Winarski D, Perssson C, Selim FA. Appl Phys Lett 2014;105:221110.
[6] Taurn M, Selim F, McCluskey M. Phys Rev Lett 2013;111:187403.
[7] Krause-Rehberg R, Leipner H. Positron annihilation in semiconductors. Springer-Verlag; 1999.
[8] Hautojaervi P. Positrons in solids. Heidelberg: Springer-Verlag; 1979.
[9] Selim F, Varney C, Taurn M, Rowe M, Collins G, McCluskey M. Phys Rev B 2013;88:174102.
[10] Varney C, Selim F. Acta Phys Polonica A 2014;125:764.
[11] Selim F. Formation and role of intrinsic defects in ZnO. In: Selim F, editor. ZnO, the future material for electronics, a comprehensive review on ZnO physics and defects. Berlin: Research Signpost; 1999.
[12] McCluskey M, Haller E. Dopants and defects in semiconductors. Taylor and Francis Group; 2012.
[13] Selim F, Wells D, Harmon J. Rev Sci Instrum 2005;76:033905.
[14] Selim F, Wells D, Harmon J, Kwofie J, Erikson G, Roney T. J Rad Phys Chem 2003;68:427.
[15] Keeble D, Mackie R, Egger W, Löwe B, Pikart P, Hugenschmidt C, Jackson T. Phys Rev B 2010;81:064102.
[16] Keeble D, Wicklein S, Dittmann R, Ravelli L, Mackie R, Egger W. Phys Rev Lett 2010;105:226102.
[17] Mackie R, Singh S, Laverock J, Dugdale S, Keeble D. Phys Rev B 2009;79:014102.
[18] Tarun M, McCluskey M. J Appl Phys 2011;109:063706.
[19] Beadie G, Rabinovich W, Wickenden A, Koleske D, Binari S, Freitas Jr J. Appl Phys Lett 1997;71:1092.
[20] Li J, Lin J, Jiang H, Geisz J, Kurtz S. Appl Phys Lett 1999;75:1899.
[21] Devor D, Pastor R, DeShazer L. J Chem Phys 1984;81:4104.
[22] Moulson A, Roberts J. Trans Br Ceram Soc 1960;59:388.